SCIENTIFIC REPORTS

Quantum phases in circuit QED with a superconducting qubit array

Yuanwei Zhang[1,2], Lixian Yu[2,3], J. -Q. Liang[1], Gang Chen[2], Suotang Jia[2] & Franco Nori[4,5,6]

[1]Institute of Theoretical Physics, Shanxi University, Taiyuan 030006, P. R. China, [2]State Key Laboratory of Quantum Optics and Quantum Optics Devices, Institute of Laser spectroscopy, Shanxi University, Taiyuan 030006, P. R. China, [3]School of Physical Science and Technology, Soochow University, Suzhou, Jiangsu 215006, P. R. China, [4]CEMS, RIKEN, Saitama 351-0198, Japan, [5]Physics Department, The University of Michigan, Ann Arbor, Michigan 48109-1040, USA, [6]Department of Physics, Korea University, Seoul 136-713, Korea.

Circuit QED on a chip has become a powerful platform for simulating complex many-body physics. In this report, we realize a Dicke-Ising model with an antiferromagnetic nearest-neighbor spin-spin interaction in circuit QED with a superconducting qubit array. We show that this system exhibits a competition between the collective spin-photon interaction and the antiferromagnetic nearest-neighbor spin-spin interaction, and then predict four quantum phases, including: a paramagnetic normal phase, an antiferromagnetic normal phase, a paramagnetic superradiant phase, and an antiferromagnetic superradiant phase. The antiferromagnetic normal phase and the antiferromagnetic superradiant phase are new phases in many-body quantum optics. In the antiferromagnetic superradiant phase, both the antiferromagnetic and superradiant orders can coexist, and thus the system possesses $Z_2^z \otimes Z_2$ symmetry. Moreover, we find an unconventional photon signature in this phase. In future experiments, these predicted quantum phases could be distinguished by detecting both the mean-photon number and the magnetization.

ircuit quantum electrodynamics (QED) based on superconducting qubits is a fascinating topic in quantum optics and quantum information[1–3]. This artificial spin-1/2 particle can be controlled by tuning the external magnetic flux and gate voltage[4–6]. Moreover, a strong spin-photon coupling has been achieved, which allows to implement quantum operations for long coherence times[7,8]. Recently, many important quantum effects in atomic physics and quantum optics have been observed in this artificial spin-photon interaction[9,10]. Particularly, experiments realized multiple superconducting qubits interacting with a transmission-line resonator[11]. These experiments allow to explore many-body phenomena via circuit QED[12–21]. For example, the challenging Dicke quantum phase transition from a normal phase to a superradiant phase, which was predicted more than 30 years ago[22–24], can be realized by controlling the gate voltage or external magnetic flux[25–28] and the no-go theorem arising from the Thomas-Reich-Ruhn sum rule may be overcome[29,30]. Moreover, the Jaynes-Cummings lattice model[31] can also be simulated by an array of transmission-line resonators, each coupled to a single artificial particle[32,33]. In addition, by measuring the microwave photon signature, the many-body none-quilibrium dynamics, as well as the known phase diagrams, could be derived[34–36].

On the other experimental side, superconducting qubits can couple with each other, forming an array with an effective nearest-neighbor spin-spin interaction[37,38]. Thus, it is meaningful to explore the many-body physics when a superconducting qubit array couples with a transmission-line resonator because there exists a competition between the collective spin-photon interaction and the nearest-neighbor spin-spin interaction. Recently, sudden switchings, as well as a bistable regime between a ferromagnetic phase and a paramagnetic phase, have been predicted[39], attributed to this competition.

In this report, we investigate the quantum phases in circuit QED with a superconducting qubit array, which is governed by a Dicke-Ising model with an antiferromagnetic nearest-neighbor spin-spin interaction. By considering the competition between the collective spin-photon interaction and the antiferromagnetic nearest-neighbor spin-spin interaction, we predict four quantum phases, including: a paramagnetic normal phase (PNP), an antiferromagnetic normal phase (ANP), a paramagnetic superradiant phase (PSP), and an antiferromagnetic superradiant phase (ASP). The ANP and the ASP are new phases in many-body quantum optics. In the ASP, both the antiferromagnetic and superradiant orders can coexist, and thus the system possesses $Z_2^z \otimes Z_2$ symmetry, i.e., both $U(1)$ and translation symmetries are broken simultaneously. Moreover, we find an unconventional photon signature in this phase which could increase from zero to a finite value and then decrease when increasing an

1

effective magnetic field. In future experiments, these predicted quantum phases could be identified by detecting both the mean-photon number and the magnetization.

Results

System and Hamiltonian. Figure 1 shows our proposed quantum network. Many superconducting qubits connected in a chain couple capacitively to their neighboring qubits and also interact identically with a one-dimensional transmission-line resonator. The corresponding Hamiltonian is given by[4–6]

$$H_1 = e^2 \sum_{i,j} \left(n_i - N_g \right)^T \bar{C}_{ij}^{-1} \left(n_j - N_g \right) - \sum_i E_J \cos \varphi_i, \quad (1)$$

where n_i is the number of Cooper pairs on the ith island,

$$N_g = \frac{C_g V_g}{2e} \quad (2)$$

is the dimensionless gate charge with gate capacitance C_g and gate voltage V_g,

$$E_J = 2E_J^0 \cos\left(\pi \frac{\Phi_x}{\Phi_0} \right) \quad (3)$$

is the tunable Josephson tunneling energy with single-junction Josephson energy E_J^0, external magnetic flux Φ_x, and magnetic flux quantum Φ_0, φ_i is the phase of the superconducting order parameter of the ith island, and $\bar{C}$ is the capacitance matrix. The element $C_{ii} = C_\Sigma$ is the total capacitance connected to the ith island and $C_{ii \pm 1} = -C$ is the coupling capacitance between two adjacent superconducting qubits. In general, the coupling capacitance C is much smaller than the total capacitance C_Σ. As a consequence, the next-nearest-neighbor term of $\bar{C}$ can be neglected safely and the Hamiltonian H_1 is rewritten as

$$H_2 = \sum_i \left[\frac{2e^2}{C_\Sigma} \left(n_i - N_g \right)^2 - E_J \cos \varphi_i \right] + \frac{4e^2 C}{C_\Sigma^2} \sum_i \left(n_i - N_g \right)\left(n_{i+1} - N_g \right). \quad (4)$$

Near the degeneracy point, only a pair of adjacent charge states ($n_i = 0$ and $n_i = 1$) on the island are relevant. If we define these charge states as the effective spin basis states $|\uparrow_i\rangle$ and $|\downarrow_i\rangle$, i.e., $|n_i = 0\rangle \leftrightarrow |\uparrow_i\rangle$ and $|n_i = 1\rangle \leftrightarrow |\downarrow_i\rangle$, the Hamiltonian H_2 reduces to the form

$$H_3 = J \sum_i \sigma_z^i \sigma_z^{i+1} + \varepsilon \sum_i \sigma_z^i - \frac{E_J}{2} \sum_i \sigma_x^i, \quad (5)$$

where $\sigma_z^i = |\uparrow_i\rangle\langle\uparrow_i| - |\downarrow_i\rangle\langle\downarrow_i|$ and $\sigma_x^i = |\uparrow_i\rangle\langle\downarrow_i| - |\downarrow_i\rangle\langle\uparrow_i|$ are the Pauli spin operators,

$$\varepsilon = 2e^2 \left(\frac{C}{C_\Sigma^2} + \frac{1}{C_\Sigma} \right)\left(N_g - \frac{1}{2} \right) \quad (6)$$

is an effective magnetic field, and

$$J = \frac{e^2 C}{C_\Sigma^2} \quad (7)$$

describes the capacitance-induced nearest-neighbor spin-spin interaction.

Now a one-dimensional transmission-line resonator is placed in parallel to the superconducting qubits. All superconducting qubits are situated at the antinode of the magnetic field induced by the oscillating supercurrent in the transmission-line resonator[2,3]. Due to the boundary condition at the end of the transmission-line resonator, these superconducting qubits are controlled only by the magnetic component, which shifts the original magnetic flux Φ_x by

$$\tilde{\Phi}_x = \Phi_x + \frac{g_0 \Phi_0}{\pi}\left(a + a^\dagger \right), \quad (8)$$

where

$$g_0 = \frac{\pi S_0}{d\Phi_0} \sqrt{\frac{\hbar l \omega}{L_0}}, \quad (9)$$

l is the inductance per unit length, and S_0 is the enclosed area of the superconducting qubit. In the Lamb-Dicke limit ($g_0 \sqrt{\langle a^\dagger a \rangle + 1} \ll 1$), together with the condition $\Phi_x = \Phi_0/2$, an effective Hamiltonian for Fig. 1 is obtained by

$$H = J \sum_i \sigma_z^i \sigma_z^{i+1} + \varepsilon \sum_i \sigma_z^i + \frac{g}{\sqrt{N}} \sum_i \sigma_x^i \left(a + a^\dagger \right) + \omega a^\dagger a, \quad (10)$$

where

$$g = \sqrt{N} E_J^0 g_0 \quad (11)$$

is the collective spin-photon coupling strength. In this Hamiltonian, all parameters can be controlled independently. For example, the effective magnetic field ε can be tuned via the gate voltage V_g from the negative to the positive. For simplicity, we address mainly the case $\varepsilon \geq 0$ in the following discussions.

The Hamiltonian (10) is a Dicke-Ising model with an antiferromagnetic nearest-neighbor spin-spin interaction. This Hamiltonian shows clearly that when both g and J coexist, the collective spin-photon interaction has a competition with the nearest-neighbor spin-spin interaction. As a result, it exhibits exotic phase transitions
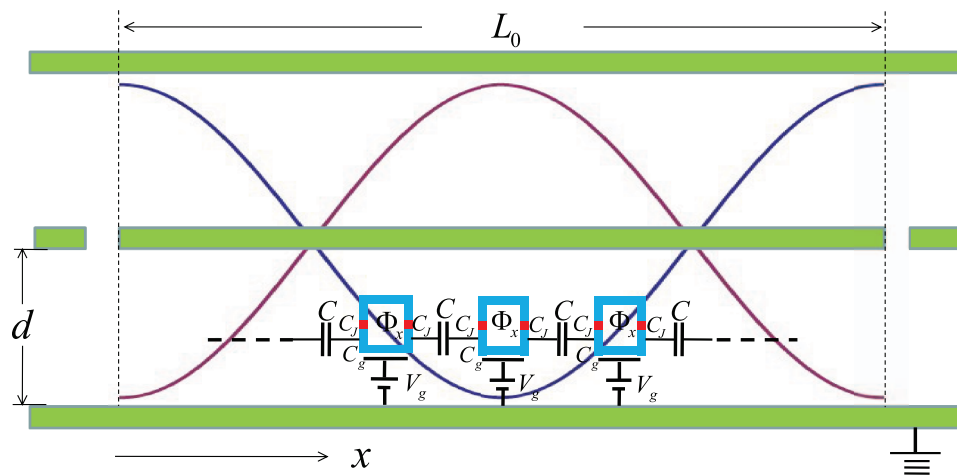

Figure 1 | Proposed circuit QED with a superconducting qubit array.

beyond the previous predictions of the standard Dicke (Ising) model. For example, a first-order superradiant phase transition has been predicted[40,41], when $J < 0$. In this report, we will find rich quantum phases including the PNP, the ANP, the PSP, and the ASP for $J > 0$.

Quantum phases. For the Hamiltonian (10), the quantum phases can be revealed by calculating the ground-state energy and the order parameters via a mean-field approach[42]. In the classical picture, the spin in the Hamiltonian (10) can be represented as a vector line in the xz plane with the unit vector $\vec{n} = (\cos\varphi, 0, \sin\varphi)$. Thus, we can introduce a variational ground-state wave function

$$|\lambda_0, \varphi\rangle = \prod_i |\varphi_i\rangle \otimes |\lambda_0\rangle, \tag{12}$$

where

$$|\varphi_i\rangle = \left[\cos\left(\frac{\pi}{4} - \frac{\varphi_i}{2}\right), \sin\left(\frac{\pi}{4} - \frac{\varphi_i}{2}\right)\right]^T \tag{13}$$

and

$$|\lambda_0\rangle = \exp\left(-\frac{\lambda_0^2}{2} + \lambda_0 a^\dagger\right)|0\rangle \tag{14}$$

are the spin and boson coherent states, to describe both the antiferromagnetic and superradiant properties.

Since the antiferromagnetic exchange interaction ($J > 0$) leads to a staggered arrangement of all spins in the z direction, we should consider two sublattices with φ_1 and $-\varphi_2$, which corresponds to the odd and even sites of spins, respectively, in the ground-state wave function. After a straightforward calculation, the scaled ground-state energy

$$E = \langle\lambda_0, \varphi_1, \varphi_2|H|\lambda_0, \varphi_1, \varphi_2\rangle/N \tag{15}$$

is given by

$$E = \omega\lambda^2 - J\sin\varphi_1\sin\varphi_2 + \frac{\varepsilon}{2}(\sin\varphi_1 - \sin\varphi_2) + g\lambda(\cos\varphi_1 + \cos\varphi_2), \tag{16}$$

where $\lambda = \lambda_0/\sqrt{N}$ and the parameters (λ, φ_1 and φ_2) are to be determined.

As shown in the Methods section, by minimizing the ground-state energy E with respect to the variational parameters (λ, φ_1, φ_2), we obtain three equilibrium equations:

$$\omega\lambda + g(\cos\alpha\cos\beta) = 0, \tag{17}$$

$$J(\sin 2\alpha - \sin 2\beta) - \varepsilon\cos(\alpha+\beta) - 2g\lambda\sin(\alpha+\beta) = 0, \tag{18}$$

$$J(\sin 2\alpha - \sin 2\beta) + \varepsilon\cos(\alpha-\beta) - 2g\lambda\sin(\alpha-\beta) = 0, \tag{19}$$

where

$$\alpha = \frac{1}{2}(\varphi_1 + \varphi_2) \in \left[-\frac{\pi}{2}, \frac{\pi}{2}\right], \tag{20}$$

$$\beta = \frac{1}{2}(\varphi_1 - \varphi_2) \in \left[-\frac{\pi}{2}, \frac{\pi}{2}\right]. \tag{21}$$

These equilibrium equations, together with the stable conditions (see the Methods section), determine the ground-state energy in Eq. (16) and the order parameters, such as the mean-photon number $\langle a^\dagger a\rangle$, the magnetization $\langle S_z\rangle$ and the staggered magnetization $\langle M_s\rangle$, which are given respectively by

$$\begin{cases} \frac{\langle a^\dagger a\rangle}{N} = \frac{g^2}{\omega^2}\cos^2\alpha\cos^2\beta \\ \frac{\langle S_z\rangle}{N} = \frac{1}{N}\left\langle\sum_i\sigma_z^i\right\rangle = \cos\alpha\sin\beta \\ \langle M_s\rangle = \frac{1}{N}\left|\sum_i(-1)^i\langle\sigma_i^z\rangle\right| = |\sin\alpha\cos\beta| \end{cases} \tag{22}$$

The introduction of the order parameter, the staggered magnetization $\langle M_s\rangle$, is to conveniently discuss the antiferromagnetic properties of the Hamiltonian (10). After the ground-state energy, and especially, the order parameters, are obtained, several rich phase diagrams can be obtained.

We first address two known limits. The first is the case when $J = 0$, in which the Hamiltonian (10) reduces to the standard Dicke model[43]

$$H_D = \varepsilon\sum_i\sigma_z^i + \frac{g}{\sqrt{N}}\sum_i\sigma_x^i(a + a^\dagger) + \omega a^\dagger a. \tag{23}$$

By means of the equilibrium equations (17)–(19) and the stable conditions, we find

$$\alpha = 0, \beta = -\frac{\pi}{2} \tag{24}$$

for $g < g_c$ and

$$\alpha = 0, \beta = -\arcsin\left[\frac{\varepsilon}{2(J + g^2/\omega)}\right] \tag{25}$$

for $g > g_c$, where $g_c = \sqrt{\varepsilon\omega/2}$, i.e.,

$$\frac{\langle a^\dagger a\rangle}{N} = 0, \frac{\langle S_z\rangle}{N} = -1 \tag{26}$$

for $g < g_c$ and

$$\frac{\langle a^\dagger a\rangle}{N} = \frac{g^2}{\omega^2} - \frac{\varepsilon^2}{4g^2}, \frac{\langle S_z\rangle}{N} = -\frac{\varepsilon\omega}{2g^2} \tag{27}$$

for $g > g_c$. This means that a second-order quantum phase transition from the normal phase ($g < g_c$) to the superradiant phase ($g > g_c$) occurs[44,45], as shown in Fig. 2(a). Moreover, the Dicke model has $U(1)$ symmetry in the normal phase. Whereas, in the superradiant phase the system acquires macroscopic collective excitations governed mainly by the collective spin-photon interaction term $g\sum_i\sigma_x^i(a + a^\dagger)$, and thus it has $Z_2^z \otimes Z_2$ symmetry, where Z_2^z is the global rotation of π around the z axis[46] and Z_2 is the change of sign of the boson coherent state ($|\lambda_0\rangle \rightarrow -|\lambda_0\rangle$). In experiments, this quantum phase transition has been observed[47–49] in an optical cavity with a Bose-Einstein condensate by measuring the mean-photon number $\langle a^\dagger a\rangle$ and the magnetization $\langle S_z\rangle/N$. Recently, it has been well investigated in many-body circuit QED[25–30] and spin-orbit-driven Bose-Einstein condensate[50].

For $g = 0$, the Hamiltonian (10) turns into the Ising model[51]

$$H_I = J\sum_i\sigma_z^i\sigma_z^{i+1} + \varepsilon\sum_i\sigma_z^i, \tag{28}$$

in which a first-order phase transition from the paramagnetic phase to the antiferromagnetic phase at the critical point $J_c = \varepsilon/2$ can be recovered. In the paramagnetic phase ($J < J_c$), the ground-state wave function is $|\dots \downarrow\downarrow\downarrow\downarrow\downarrow\downarrow\downarrow\downarrow \dots\rangle$, which implies that the system has translation symmetry and $\langle S_z\rangle/N = -1$ and $\langle M_s\rangle = 0$. In the antiferromagnetic phase ($J > J_c$), the ground-state wave function becomes $|\dots \uparrow\downarrow\uparrow\downarrow\uparrow\downarrow\uparrow\downarrow \dots\rangle$, in which translation symmetry is broken and $\langle S_z\rangle/N = 0$ and $\langle M_s\rangle = 1$.

If both g and J are non-zeros, we find four different regions: (i) $\alpha = 0$, $\beta = -\pi/2$, (ii) $\alpha = +\pi/2$, $\beta = 0$, (iii) $\alpha = 0$, $\beta \neq 0$, and (iv) $\alpha \neq 0$, $\beta \neq 0$. Specially, the order parameters in these four regions are given respectively by
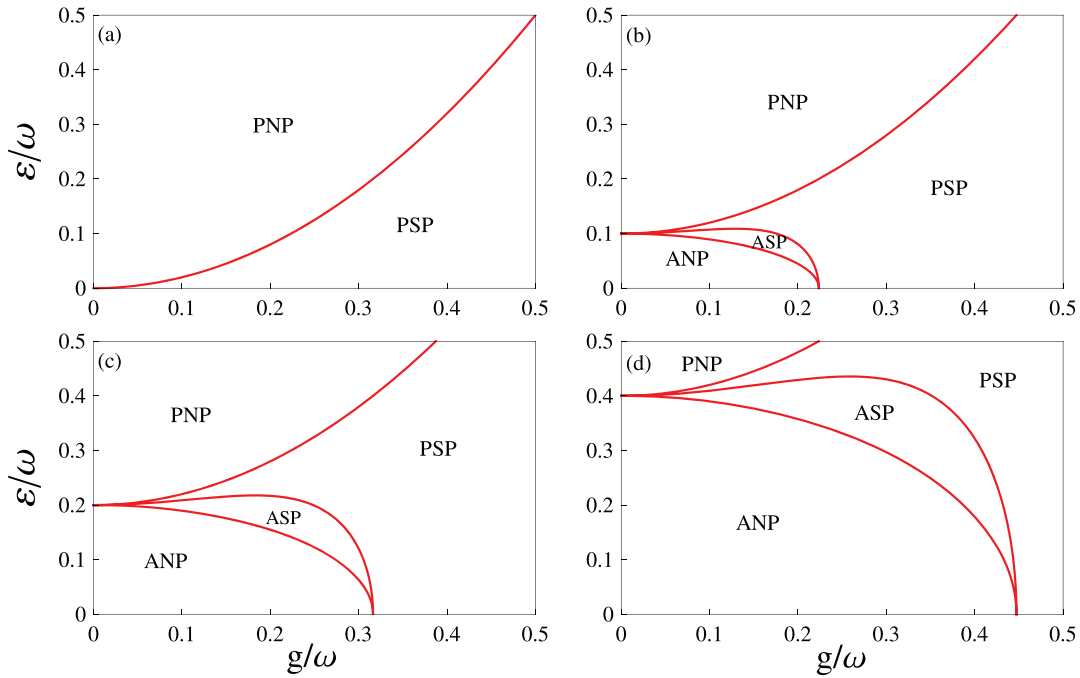
Figure 2 | Phase diagrams for different antiferromagnetic spin-spin nearest-neighbor interactions. The plotted parameters are chosen as (a) $J/\omega = 0$, (b) $J/\omega = 0.05$, (c) $J/\omega = 0.1$, and (d) $J/\omega = 0.2$, respectively. In (b), (c) and (d), the phase boundaries (from top to bottom) are determined respectively by $\varepsilon_c = 2(J + g^2/\omega)$, $\varepsilon_c = 2(J + g^2/\omega)\sqrt{1 - g^2/\omega J}$, and $\varepsilon_c = 2J\sqrt{1 - g^2/\omega J}$.

$$\text{(i)} \quad \frac{\langle a^\dagger a \rangle}{N} = 0, \frac{\langle S_z \rangle}{N} = -1, \langle M_s \rangle = 0, \tag{29}$$

$$\text{(ii)} \quad \frac{\langle a^\dagger a \rangle}{N} = 0, \frac{\langle S_z \rangle}{N} = 0, \langle M_s \rangle = 1, \tag{30}$$

$$\text{(iii)} \frac{\langle a^\dagger a \rangle}{N} = \frac{g^2}{\omega^w}\left[1 - \frac{\varepsilon^2}{4\left(J + \frac{g^2}{\omega}\right)^2}\right], \frac{\langle S_z \rangle}{N} = -\frac{\varepsilon}{2\left(J + \frac{g^2}{\omega}\right)}, \langle M_s \rangle = 0, \tag{31}$$

$$\text{(v)} \frac{\langle a^\dagger a \rangle}{N} = \frac{g^2}{\omega^w}\cos^2\alpha\cos^2\beta, \frac{\langle S_z \rangle}{N} = \cos\alpha\sin\beta, \langle M_s \rangle = |\sin\alpha\cos\beta|, \tag{32}$$

where

$$\cos\alpha = \frac{-\varepsilon\sin\beta}{2(J - g^2\cos^2\beta/\omega)}, \tag{33}$$

$$\cos^2\beta = \frac{\omega}{g^2}\left[J - \frac{\varepsilon}{2}\sqrt{1 - \frac{g^2}{\omega J}}\right]. \tag{34}$$

In terms of the different properties of the order parameters, the cases (i)–(iv) are denoted by PNP, ANP, PSP, and ASP, respectively. The ANP ($\langle a^\dagger a \rangle/N = 0$, $\langle S_z \rangle/N = 0$ and $\langle M_s \rangle = 1$) and the ASP ($\langle a^\dagger a \rangle/N \neq 0$, $\langle S_z \rangle/N \neq -1$ and $\langle M_s \rangle \neq 1$) are new phases in many-body quantum optics. In Fig. 2, we plot phase diagrams for different antiferromagnetic spin-spin nearest-neighbor interactions. This figure shows clearly that these predicted quantum phases can be driven by the collective spin-photon coupling strength g, the antiferromagnetic nearest-neighbor spin-spin interaction J, and the effective magnetic field ε. Especially, the region of the ASP becomes larger when increasing J.

In Fig. 3, we plot phase diagrams as functions of the antiferromagnetic nearest-neighbor spin-spin interaction J and the collective spin-photon coupling strength g for different effective magnetic fields (a) $\varepsilon = 0$ and (b) $\varepsilon = \omega/4$. In the absence of ε, Eq. (10) reduces to the form

$$H = J\sum_i \sigma_z^i\sigma_z^{i+1} + \frac{g}{\sqrt{N}}\sum_i \sigma_x^i(a + a^\dagger) + \omega a^\dagger a. \tag{35}$$

In such a case, only the ANP and the PSP can be found, as shown in Fig. 3(a). When increasing ε, four quantum phases are predicted again, as shown in Fig. 3(b). In addition, by means of the ground-state energy, we find that all transitions between these different quantum phases in Figs. 2 and 3 are of second order.

Symmetry. In order to better understand these predicted quantum phases, it is necessary to discuss the corresponding symmetries. For the PNP and the PSP, the system properties are similar to those of the normal phase and the superradiant phase in the standard Dicke model, i.e., the system displays both $U(1)$ and translation symmetries in the PNP, and becomes $Z_2^z \otimes Z_2$ and translation symmetries in the PSP. However, in the ANP, though no photon is excited, the antiferromagnetic order emerges. This implies that in such a case only $U(1)$ symmetry can be found. Interestingly, in the ASP the Hamiltonian (10) is governed mainly by the term

$$H_{gJ} = J\sum_i \sigma_z^i\sigma_z^{i+1} + \frac{g}{\sqrt{N}}\sum_i \sigma_x^i(a + a^\dagger) \tag{36}$$

in which there exists a competition between the antiferromagnetic nearest-neighbor spin-spin interaction and the collective spin-photon interaction. As a result, both the antiferromagnetic and superradiant orders coexist and the system possesses $Z_2^z \otimes Z_2$ symmetry, i.e., both $U(1)$ and translation symmetries are broken simultaneously.

Possible experimental observation. We first estimate the parameters for experiments. When we choose $C_\Sigma \sim 600$ aF, $C \sim 20$ aF, $E_J^0 \sim 2\pi \times 3.5$ GHz, $S_0 \sim 1$ μm², $d \sim 10$ μm, $L_0 \sim 19$ mm,
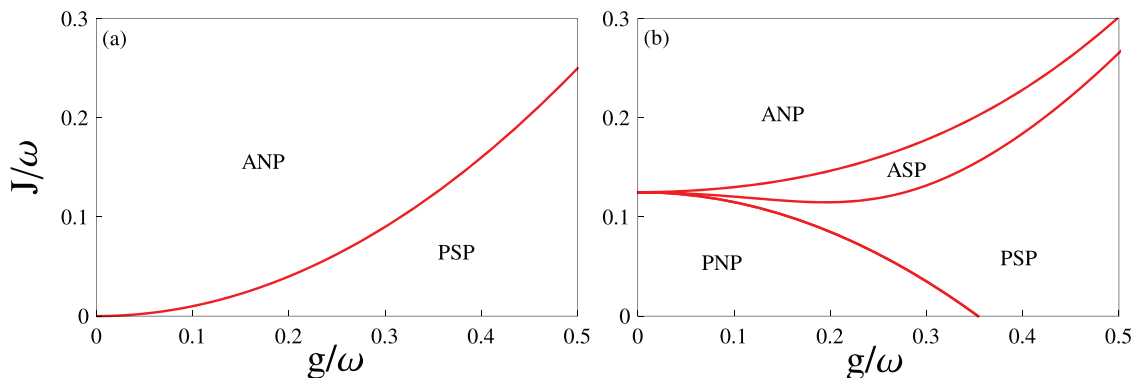
Figure 3 | Phase diagrams for different effective magnetic fields. The plotted parameters are chosen as (a) $\varepsilon/\omega = 0$ and (b) $\varepsilon/\omega = 0.25$, respectively. In (a), the phase boundary is determined by $J_c = g^2/\omega$. In (b), the phase boundaries (from top to bottom) are given respectively by $J_c = \left(g^2/\omega + \sqrt{\varepsilon^2 + g^4/\omega^2}\right)\Big/2$, $\left(J_c + g^2/\omega\right)\sqrt{1 - g^2/(\omega J_c)} = \varepsilon/2$, and $J_c = \varepsilon/2 - g^2/\omega$.

$\omega \sim 2\pi \times 6.729$ GHz, and $N = 100$[11], the antiferromagnetic nearest-neighbor spin-spin interaction parameter and the collective spin-photon coupling strength are given respectively by $J \sim 2\pi \times 2.2$ GHz and $g \sim 2\pi \times 1.5$ GHz ($g_0 = 0.01$ is responsible for the Lamb-Dicke approximation). In addition, the effective magnetic field ε can range from 0 to $2\pi \times 6.8$ GHz by controlling the gate voltage V_g. These parameters ensure that the system should probe the predicted phase transitions. To observe these phase transitions, the relaxation time T_1 and the coherence time T_2 should be much smaller than the lifetime $1/\kappa$ of the photon, i.e., $T_1 > T_2 > 1/\kappa = 23.4$ ns, where κ is the decay rate of the photon. This restriction can be easy to satisfy in current experimental setups (for example, $T_1 = 7.3$ μs and $T_2 = 500$ ns in Ref. 52).

We now illustrate how to identify these different quantum phases. Here we propose to detect four phases by measuring both the mean-photon number $\langle a^\dagger a\rangle$ and the magnetization $\langle S_z\rangle$. For the PNP and the ANP, we can separate these by directly observing the magnetization because $\langle S_z\rangle/N = -1$ in the PNP and $\langle S_z\rangle/N = 0$ in the ANP, as shown in Fig. 4(a). For the PSP and the ASP, both the photon and the spin are collectively excited. Moreover, when increasing the effective magnetic field ε, $\langle S_z\rangle/N$ always decreases. This means that it is difficult to distinguish the PSP and the ASP by measuring $\langle S_z\rangle/N$. Fortunately, we find that in the ASP the mean-photon number has an unconventional behavior that could increase it from zero to a finite value and then decrease, as shown in Fig. 4(b). The relevant

physics can be understood as follows. When the effective magnetic field ε is applied, it can initially promote the arrangement of all spins from the antiferromagnetic to the paramagnetic terms[53]. For example, in the case of a weak ε, the spin arrangement becomes $|\ldots \uparrow\downarrow\uparrow \{\downarrow\downarrow\downarrow\} \uparrow\downarrow\uparrow \ldots\rangle$ from the antiferromagnetic case $|\ldots \uparrow\downarrow\uparrow\downarrow\uparrow\downarrow\uparrow\downarrow \ldots\rangle$. This process is helpful for achieving photon-induced collective excitations. Thus, the mean-photon number can increase. However, the rearrangement of spins gives rise to an opposite result of the magnetization, i.e., it decreases when increasing ε. For strong ε, this effective magnetic field in the z axis leads to a large spin imbalance $|\ldots \uparrow\uparrow\downarrow\downarrow\downarrow\downarrow\downarrow \ldots\rangle$ and thus suppresses the spin-photon collective excitations, i.e., both $\langle a^\dagger a\rangle/N$ and $\langle S_z\rangle/N$ decrease when increasing ε. In terms of the different behaviors of both $\langle a^\dagger a\rangle/N$ and $\langle S_z\rangle/N$, we argue that our predicted quantum phases can be identified.

It should be pointed out that the microwave photon in superconducting circuits is not easy to measure directly[54] via photon-number detectors, because its energy ($\hbar\omega$) is very small. However, in the dispersive region $\Delta \gg g$, where $\Delta = \varepsilon - \omega$, the photon number can be detected by the photon-number-dependent light shift (the Stark plus Lamb shifts) of the atom transition frequency[55]. Unfortunately, to achieve the predicted phase diagrams, the system should work at the quasi-dispersive-strong region $\Delta/g < 4$. In such a region, the above approach to detect photons does not work. Recently, it has been proposed[56,57] to detect the photon by irreversible absorption of photons. In these proposals[56,57], the absorbers along the waveguide are built with bistable quantum circuits, and can produce a large voltage pulse when the photon decays into a stable state. This suggests that in future experiments the mean-photon number could be detected, and then our predicted phase diagrams could also be observed.

Discussion

Let us here address the no-go theorem in quantum optics. This no-go theorem, demonstrated[58] in 1975, shows that in a typical optical cavity with an ensemble of natural two-level atoms, the phase transition from the normal phase to the superradiant phase is forbidden by the A^2 term, where A is the vector potential. Recently, the no-go theorem has been addressed[29,30] in circuit QED, with many superconducting qubits interacting with a quantized voltage (microwave photon). However, in this report, the required microwave photon is generated from the quantization of the magnetic flux. In such a case, no A^2 term can occur, i.e., the no-go theorem is not valid.

We now consider how the decay of the photon and the disorder in fabrication affect the predicted phase diagrams. When considering the decay of the photon, the stationary mean-photon number, which can be derived from
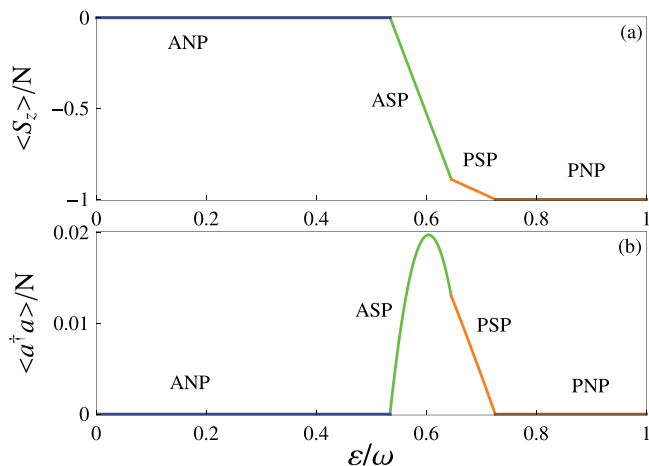
Figure 4 | Order parameters versus the effective magnetic field. In (a) and (b), the magnetization $\langle S_z\rangle/N$ and the mean-photon number $\langle a^\dagger a\rangle/N$ as functions of the effective magnetic field ε are plotted, respectively, when $J/\omega = 0.30$ and $g/\omega = 0.25$.
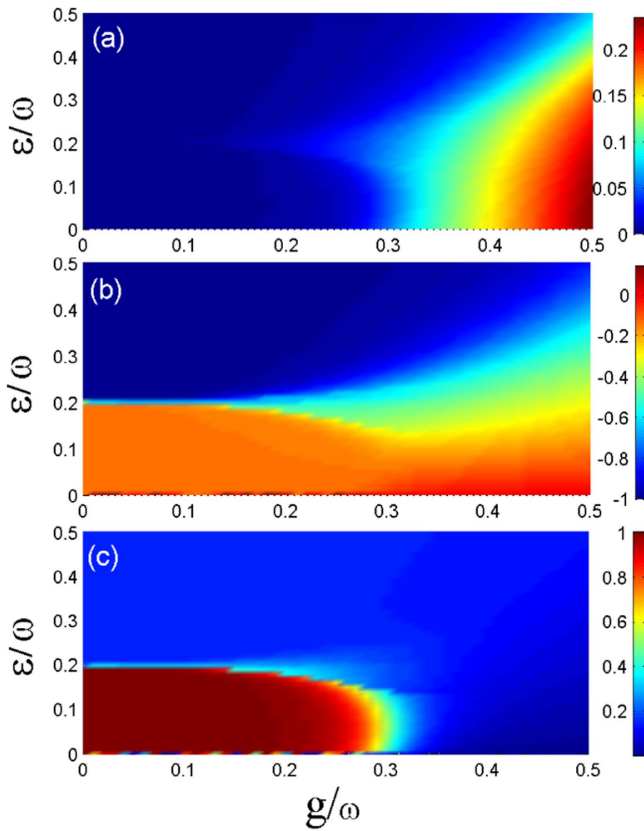
Figure 5 | Order parameters via the direct numerical diagonalization method. In (a)–(c), the mean-photon number $\langle a^\dagger a\rangle/N$, the magnetization $\langle S_z\rangle/N$, and the the staggered magnetization $\langle M_s\rangle$ as functions of the collective spin-photon coupling strength g and the effective magnetic field ε are plotted, respectively, when $J/\omega = 0.1$ and $N = 7$.

$$i\frac{\partial a}{\partial t} = \omega a + \frac{g}{\sqrt{N}}S_x - i\kappa a = 0, \tag{37}$$

becomes

$$\langle a^\dagger a\rangle = \frac{g^2}{N(\omega^2 + \kappa^2)}\langle S_x\rangle^2, \tag{38}$$

whereas the stationary value of $\langle S_x\rangle$ remains unchanged (i.e., it is identical to the case without photon decay). This means that we can use an effective Hamiltonian

$$H_{\text{eff}} = J\sum_i \sigma_z^i \sigma_z^{i+1} + \frac{g}{\sqrt{N}}\sum_i \sigma_x^i(a + a^\dagger) + \omega_{\text{eff}} a^\dagger a, \tag{39}$$

with

$$\omega_{\text{eff}} = \sqrt{\omega^2 + \kappa^2}, \tag{40}$$

to discuss the phase diagrams[49] induced by the decay of the photon. Since the decay rate κ of the photon ($\sim$MHz) is far smaller than the other parameters ($\sim$GHz), the decay of the photon has almost no effect on the predicted phase diagrams.

In addition, the imperfections in fabrication result in a weak randomness in the antiferromagnetic nearest-neighbor spin-spin interaction[14]. Moreover, the disorder antiferromagnetic interaction generates a disordered phase, such as a random singlet phase[59]. In this phase, most spins form a singlet pair with nearby spins, and the residual induce weak long-distance pairs. Unfortunately, the disordered phase is only a local correlation, and is thus unstable in

the presence of a strong external magnetic field (i.e., for a weak magnetic field, the disordered phase can occur). The phase diagrams predicted here should be observable under a strong magnetic field (See Figs. 2(c) and 2(d)). This means that these predicted quantum phases will not be qualitatively affected by weak disorder.

Mean-field predictions become more accurate for larger number of spins. However, mean-field is often a good starting point, and provides some basic insight in the system. Moreover, for current experimental techniques, the spin number is not sufficiently large, but this should change in the future. For smaller number of spins, we can perform direct numerical diagonalization to discuss the ground-state properties. In Fig. 5, we plot the order parameters $\langle a^\dagger a\rangle/N$, $\langle S_z\rangle/N$, and $\langle M_s\rangle$ as functions of the collective spin-photon coupling strength g and the effective magnetic field ε. This result shows clearly that for a small number of spins, the predicted quantum phases still exist, but the phase boundaries are affected significantly.

In summary, we have investigated the Dicke-Ising model with an antiferromagnetic nearest-neighbor spin-spin interaction in circuit QED for a superconducting qubit array and predicted four quantum phases, including the PNP, the ANP, the PSP and the ASP, with different symmetries. Moreover, all transitions between these different quantum phases are of second order. We have also found an unconventional photon signature in the ASP, where both the antiferromagnetic and superradiant orders coexist. We believe that this system allows to explore exotic many-body physics in quantum optics and condensed-matter physics because it has an interesting competition between the collective spin-photon interaction and the nearest-neighbor spin-spin interaction.

Methods

Three equilibrium equations and the corresponding stable conditions. Here we present detailed calculations on how to derive the three equilibrium equations (17)–(19) and the corresponding stable conditions. After minimizing the ground-state energy E in Eq. (16) with respect to the variational parameters (λ, φ_1 and φ_2), we obtain three equations:

$$\frac{\partial E}{\partial\lambda} = 2\omega\lambda + g(\cos\varphi_1 + \cos\varphi_2) = 0, \tag{41}$$

$$\frac{\partial E}{\partial\varphi_1} = -J\cos\varphi_1\sin\varphi_2 + \frac{\varepsilon}{2}\cos\varphi_1 - g\lambda\sin\varphi_1 = 0, \tag{42}$$

$$\frac{\partial E}{\partial\varphi_2} = -J\sin\varphi_1\cos\varphi_2 + \frac{\varepsilon}{2}\cos\varphi_2 - g\lambda\sin\varphi_2 = 0. \tag{43}$$

After defining $\alpha = (\varphi_1 + \varphi_2)/2 \in [-\pi/2, \pi/2]$ and $\beta = (\varphi_1 - \varphi_2)/2 \in [-\pi/2, \pi/2]$, the three equilibrium equations (17)–(19) are easily derived.

In addition, by means of three parameters (λ, α and β), the ground-state stability is determined by the 3×3 Hessian matrix

$$\mathcal{M} = \begin{bmatrix} \dfrac{\partial^2 E}{\partial\lambda^2} & \dfrac{\partial^2 E}{\partial\lambda\partial\alpha} & \dfrac{\partial^2 E}{\partial\lambda\partial\beta} \\[2mm] \dfrac{\partial^2 E}{\partial\alpha\partial\lambda} & \dfrac{\partial^2 E}{\partial\alpha^2} & \dfrac{\partial^2 E}{\partial\alpha\partial\beta} \\[2mm] \dfrac{\partial^2 E}{\partial\beta\partial\lambda^2} & \dfrac{\partial^2 E}{\partial\beta\partial\alpha^2} & \dfrac{\partial^2 E}{\partial\beta^2} \end{bmatrix}. \tag{44}$$

If $\mathcal{M}$ is positive definite (i.e., all eigenvalues h_i of $\mathcal{M}$ are positive), the system is located at the stable phases. If $\mathcal{M}$ is negative definite (i.e., all eigenvalues h_i of $\mathcal{M}$ are negative), the system is unstable.

1. You, J. Q. & Nori, F. Quantum information processing with superconducting qubits in a microwave field. *Phys. Rev. B* **68**, 064509 (2003).
2. Blais, A., Huang, R.-S., Wallraff, A., Girvin, S. M. & Schoelkopf, R. J. Cavity quantum electrodynamics for superconducting electrical circuits: An architecture for quantum computation. *Phys. Rev. A* **69**, 062320 (2004).
3. Wallraff, A. *et al.* Strong coupling of a single photon to a superconducting qubit using circuit quantum electrodynamics. *Nature* **431**, 162 (2004).

4. You, J. Q. & Nori, F. Superconducting circuits and quantum information. *Phys. Today* **58**(11), 42 (2005).

5. Schoelkopf, R. J. & Girvin, S. M. Wiring up quantum systems. *Nature* **451**, 664–669 (2008).

6. Clarke, J. & Wilhelm, F. K. Superconducting quantum bits. *Nature* **453**, 1031–1042 (2008).

7. Buluta, I., Ashhab, S. & Nori, F. Natural and artificial atoms for quantum computation. *Rep. Prog. Phys.* **74**, 104401 (2011).

8. Xiang, Z.-L., Ashhab, S., You, J. Q. & Nori, F. Hybrid quantum circuits: Superconducting circuits interacting with other quantum systems. *Rev. Mod. Phys.* **85**, 623 (2013).

9. Buluta, I. & Nori, F. Quantum simulators. *Science* **326**, 108–111 (2009).

10. You, J. Q. & Nori, F. Atomic physics and quantum optics using superconducting circuits. *Nature* **474**, 589–597 (2011).

11. Fink, J. M. *et al.* Dressed collective qubit states and the Tavis-Cummings model in circuit QED. *Phys. Rev. Lett.* **103**, 083601 (2009).

12. Koch, J., Houck, A. A., Hur, K. L. & Girvin, S. M. Time-reversal-symmetry breaking in circuit-QED-based photon lattices. *Phys. Rev. A* **82**, 043811 (2010).

13. Hu, Y. & Tian, L. Deterministic generation of entangled photons in superconducting resonator arrays. *Phys. Rev. Lett.* **106**, 257002 (2011).

14. Houck, A. A., Türeci, H. E. & Koch, J. On-chip quantum simulation with superconducting circuits. *Nature Phys.* **8**, 292–299 (2012).

15. Nissen, F. *et al.* Nonequilibrium dynamics of coupled qubit-cavity arrays. *Phys. Rev. Lett.* **108**, 233603 (2012).

16. Marcos, D., Tomadin, A., Diehl, S., & Rabl, P. Photon condensation in circuit quantum electrodynamics by engineered dissipation. *New J. Phys.* **14**, 055005 (2012).

17. Hohenadler, M., Aichhorn, M., Pollet, L. & Schmidt, S. Polariton Mott insulator with trapped ions or circuit QED. *Phys. Rev. A* **85**, 013810 (2012).

18. Underwood, D. L., Shanks, W. E., Koch, J. & Houck, A. A. Low-disorder microwave cavity lattices for quantum simulation with photons. *Phys. Rev. A* **86**, 023837 (2012).

19. Jin, J., Rossini, D., Fazio, R., Leib, M. & Hartmann, M. J. Photon solid phases in driven arrays of nonlinearly coupled cavities. *Phys. Rev. Lett.* **110**, 163605 (2013).

20. Nissen, F., Fink, J. M., Mlynek, J. A., Wallraff, A. & Keeling, J. Collective suppression of linewidths in circuit QED. *Phys. Rev. Lett.* **110**, 203602 (2013).

21. Mei, F., Stojanovic, V. M., Siddiqi, I. & Tian, L. Analog superconducting quantum simulator for Holstein polarons. *arXiv: 1307.0906* (2013).

22. Hepp, K. & Lieb, E. H. On the superradiant phase transition for molecules in a quantized radiation field: The Dicke maser model. *Ann. Phys. (N. Y.)* **76**, 360–404 (1973).

23. Wang, Y. K. & Hioes, F. T. Phase transition in the Dicke model of superradiance. *Phys. Rev. A* **7**, 831–836 (1973).

24. Hioes, F. T. & Hioes, F. T. Phase transitions in some generalized Dicke models of superradiance. *Phys. Rev. A* **8**, 1440–1445 (1973).

25. Chen, G., Chen, Z. & Liang, J. Simulation of the superradiant quantum phase transition in the superconducting charge qubits inside a cavity. *Phys. Rev. A* **76**, 055803 (2007).

26. Lambert, N., Chen, Y.-N., Johansson, R. & Nori, F. Quantum chaos and critical behavior on a chip. *Phys. Rev. B* **80**, 165308 (2009).

27. Nataf, P. & Ciuti, C. Vacuum degeneracy of a circuit QED system in the ultrastrong coupling regime. *Phys. Rev. Lett.* **104**, 023601 (2010).

28. Ian, H., Liu, Y.-X. & Nori, F. Excitation spectrum for an inhomogeneously dipole-field-coupled superconducting qubit chain. *Phys. Rev. A* **85**, 053833 (2012).

29. Nataf, P. & Ciuti, C. No-go theorem for superradiant quantum phase transitions in cavity QED and counter-example in circuit QED. *Nature Comm.* **1**, 72 (2010).

30. Viehmann, O., Delft, J. V. & Marquardt, F. Superradiant phase transitions and the standard description of circuit QED. *Phys. Rev. Lett.* **107**, 113602 (2011).

31. Greentree, A. D., Tahan, C., Cole, J. H. & Hollenberg, L. C. L. Quantum phase transitions of light. *Nature Phys.* **2**, 856–861 (2006).

32. Angelakis, D. G., Santos, M. F. & Bose, S. Photon-blockade-induced mott transitions and XY spin models in coupled cavity arrays. *Phys. Rev. A* **76**, 031805(R) (2007).

33. Hartmann, M. J., Brandão, F. & Plenio, M. Quantum many-body phenomena in coupled cavity arrays. *Laser Photonics Rev.* **2**, 527 (2008).

34. Wang, Y.-D., Xue, F., Song, Z. & Sun, C.-P. Detection mechanism for quantum phase transition in superconducting qubit array. *Phys. Rev. B* **76**, 174519 (2007).

35. Viehmann, O., von Delft, J. & Marquardt, F. Observing the nonequilibrium dynamics of the quantum transverse-field Ising chain in circuit QED. *Phys. Rev. Lett.* **110**, 030601 (2013).

36. Viehmann, O., von Delft, J. & Marquardt, F. The quantum transverse-field Ising chain in circuit quantum electrodynamics: effects of disorder on the nonequilibrium dynamics. *New J. Phys.* **15**, 035013 (2013).

37. Pashkin, Y. A. *et al.* Quantum oscillations in two coupled charge qubits. *Nature* **421**, 823–826 (2003).

38. Johnson, M. W. *et al.* Quantum annealing with manufactured spins. *Nature* **473**, 194–198 (2011).

39. Tian, L. Circuit QED and sudden phase switching in a superconducting qubit array. *Phys. Rev. Lett.* **105**, 167001 (2010).

40. Lee, C. F. & Johnson, N. F. First-order superradiant phase transitions in a multiqubit cavity system. *Phys. Rev. Lett.* **93**, 083001 (2004).

41. Gammelmark, S. & Mølmer, K. Phase transitions and Heisenberg limited metrology in an Ising chain interacting with a single-mode cavity field. *New J. Phys.* **13**, 053035 (2011).

42. Sachdev, S. *Quantum Phase Transitions.* (Cambridge University Press, Cambridge, England, 1999).

43. Dicke, R. H. Coherence in spontaneous radiation processes. *Phys. Rev.* **93**, 99–110 (1954).

44. Emary, C. & Brandes, T. Chaos and the quantum phase transition in the Dicke model. *Phys. Rev. E* **67**, 066203 (2003).

45. Chen, G., Wang, X., Liang, J.-Q & Wang, Z. D. Exotic quantum phase transitions in a Bose-Einstein condensate coupled to an optical cavity. *Phys. Rev. A* **78**, 023634 (2008).

46. Kennedy, T. & Tasaki, H. Hidden $Z_2\_Z_2$ symmetry breaking in Haldane-gap antiferromagnets. *Phys. Rev. B* **45**, 304–307 (1992).

47. Baumann, K., Guerlin, C., Brennecke, F. & Esslinger, T. Dicke quantum phase transition with a superfluid gas in an optical cavity. *Nature* **464**, 1301–1306 (2010).

48. Baumann, K., Mottl, R., Brennecke, F. & Esslinger, T. Exploring symmetry breaking at the Dicke quantum phase transition. *Phys. Rev. Lett.* **107**, 140402 (2011).

49. Ritsch, H., Domokos, P., Brennecke, F. & Esslinger, T. Cold atoms in cavity-generated dynamical optical potentials. *Rev. Mod. Phys.* **85**, 553 (2013).

50. Zhang, Y., Chen, G. & Zhang, C. Tunable spin-orbit coupling and quantum phase transition in a trapped Bose-Einstein condensate. *Sci. Rep.* **3**, 1937 (2013).

51. Ovchinnikov, A. A., Dmitriev, D. V., Krivnov, V. Ya.& Cheranovskii, V. O. Antiferromagnetic Ising chain in a mixed transverse and longitudinal magnetic field. *Phys. Rev. B* **68**, 214406 (2003).

52. Wallraff, A. *et al.* Approaching qubit with dispersive readout. *Phys. Rev. Lett.* **95**, 060501 (2005).

53. Simon, J. *et al.* Quantum simulation of antiferromagnetic spin chains in an optical lattice. *Nature* **472**, 307–312 (2011).

54. Nation, P. D., Johansson, J. R., Blencowe, M. P. & Nori, F. Stimulating uncertainty: amplifying the quantum vacuum with superconducting circuits. *Rev. Mod. Phys.* **84**, 1 (2012).

55. Schuster, D. I. *et al.* Resolving photon number states in a superconducting circuit. *Nature* **445**, 515–518 (2007).

56. Romero, G., Carcía-Rioll, J. J. & Solano, E. Microwave photon detector in circuit QED. *Phys. Rev. Lett.* **102**, 173602 (2009).

57. Chen, Y. F. *et al.* Microwave photon counter based on josephson junctions. *Phys. Rev. Lett.* **107**, 217401 (2011).

58. Rzażewski, K., Wódkiewicz, K. & Żakowicz, W. Phase transitions, two-level atoms, and the A2 term. *Phys. Rev. Lett.* **35**, 432–434 (1975).

59. Fisher, D. S. Random antiferromagnetic quantum spin chains. *Phys. Rev. B* **50**, 3799–3821 (1994).

Acknowledgments

Author contributions

G.C., S.J. and F.N. conceived the idea. Y.Z., L.Y. and J.-Q.L. performed the calculation. G.C., S.J. and F.N. wrote the manuscript.

Additional information